

# SCIENTIFIC REPORTS



OPEN

## A novel WS<sub>2</sub> nanowire-nanoflake hybrid material synthesized from WO<sub>3</sub> nanowires in sulfur vapor

Received: 21 September 2015  
 Accepted: 06 April 2016  
 Published: 16 May 2016

Georgies Alene Asres<sup>1</sup>, Aron Dombovari<sup>1</sup>, Teemu Sipola<sup>1</sup>, Robert Puskás<sup>2</sup>, Akos Kukovecz<sup>2,3</sup>, Zoltán Kónya<sup>2,4</sup>, Alexey Popov<sup>5</sup>, Jhih-Fong Lin<sup>1</sup>, Gabriela S. Lorite<sup>1</sup>, Melinda Mohl<sup>1</sup>, Geza Toth<sup>1</sup>, Anita Lloyd Spetz<sup>1,6</sup> & Krisztian Kordas<sup>1</sup>

In this work, WS<sub>2</sub> nanowire-nanoflake hybrids are synthesized by the sulfurization of hydrothermally grown WO<sub>3</sub> nanowires. The influence of temperature on the formation of products is optimized to grow WS<sub>2</sub> nanowires covered with nanoflakes. Current-voltage and resistance-temperature measurements carried out on random networks of the nanostructures show nonlinear characteristics and negative temperature coefficient of resistance indicating that the hybrids are of semiconducting nature. Bottom gated field effect transistor structures based on random networks of the hybrids show only minor modulation of the channel conductance upon applied gate voltage, which indicates poor electrical transport between the nanowires in the random films. On the other hand, the photo response of channel current holds promise for cost-efficient solution process fabrication of photodetector devices working in the visible spectral range.

Metal chalcogenides have opened unexpected opportunities for novel multifunctional materials with potential application in nano and optoelectronics. In particular, nanostructures of group 4–6 transition metal dichalcogenides (TMDCs) are recently getting an enormous attention due to their two-dimensional graphene-like layered structure and semiconducting behavior<sup>1–3</sup>. The band gap of dichalcogenides shows a systematic decrease with the increasing metallic nature of the chalcogen following the series in the main group 6 elements as S, Se and Te. However, when decreasing the number of layers in TMDCs, the band gap increases, e.g. 1.4 eV (bulk) to 2.1 eV (single layer) for WS<sub>2</sub>. Since the band gap values of TMDCs are comparable to that of Si (1.1 eV), transistor structures with similar low voltage operation are expected. As demonstrated lately, extremely high on/off channel current ratios (e.g. 10<sup>5</sup> for flakes of WS<sub>2</sub><sup>4</sup>, 10<sup>7</sup> for WS<sub>2</sub> flakes sandwiched between h-BN sheets<sup>5</sup>, and 10<sup>8</sup> for MoS<sub>2</sub> monolayers<sup>6</sup>) can be achieved without impurity doping or any particular band gap engineering, unlike in gapless graphene. Another interesting feature of several TMDCs is the switch from indirect band-to-band transition of multi-layered materials to direct gap when dealing with single-layer sheets. Accordingly, single-layer TMDCs may show photoluminescence<sup>7</sup>, which is particularly interesting for novel devices in optoelectronics<sup>8,9</sup> and sensing<sup>10</sup>.

Chemical<sup>11–13</sup> and mechanical<sup>14,15</sup> exfoliation methods are the two most commonly used techniques to produce single or few-layered dichalcogenides. Chemical exfoliation is based on an insertion of ions (typically Li<sup>+</sup>) in the layered material to make the adjacent sulfide layers more separated or expanded (chemical intercalation) by which the van der Waals interaction is weakened. Then a mechanical force is applied (e.g. sonication) to separate the intercalated layers that become suspended in the solvent in the form of mono or few-layered flakes<sup>16,17</sup>. Mechanical exfoliation proceeds in a similar vein as first described for graphene synthesis<sup>18</sup>, i.e. by peel-off from bulk or multi-layered crystals. The TMDC crystal is repeatedly cleaved using e.g. scotch tape until a very thin layer of the materials remains on the surface of the tape, from which the atomically thin films are transferred to

<sup>1</sup>Microelectronics and Materials Physics Laboratories, Department of Electrical Engineering, University of Oulu, P.O. Box 4500, FI-90014 Oulu, Finland. <sup>2</sup>Department of Applied and Environmental Chemistry, University of Szeged, Rerrich Bela ter 1, H-6720 Szeged, Hungary. <sup>3</sup>MTA-SZTE "Lendület" Porous Nanocomposites Research Group, Rerrich Bela ter 1, H-6720 Szeged, Hungary. <sup>4</sup>MTA-SZTE Reaction Kinetics and Surface Chemistry Research Group, Rerrich Bela ter 1 H-6720 Szeged, Hungary. <sup>5</sup>Optoelectronics and Measurement Techniques Laboratory, Department of Electrical Engineering, University of Oulu, P.O. Box 4500, FI-90014 Oulu, Finland. <sup>6</sup>Department of Physics, Chemistry and Biology, Linköping University, SE-58183 Linköping, Sweden. Correspondence and requests for materials should be addressed to K.K. (email: lapy@ee.oulu.fi)

a target substrate<sup>19</sup>. The synthesis of other types of dichalcogenides is described in detail elsewhere for interested readers<sup>20,21</sup>.

Both mechanical and chemical exfoliation methods are tedious, and the immobilization of individual single TMDC flakes on chips for testing or to produce devices for commercial purposes is cumbersome. Accordingly, robust methods to fabricate nanoflakes of TMDCs would help in the practical exploitation of these fascinating materials. In this work, we discuss the synthesis of WS<sub>2</sub> nanowires and nanowire-nanoflake hybrid materials by a simple single-step sulfurization from hydrothermally grown WO<sub>3</sub> nanowires. The geometry of the prepared nanostructure is novel, as the flakes reside directly on the surface of nanowires and are a direct continuation of the nanowire crystal structure. This direct crystallographic interconnection between two dimensional and one dimensional structures hold the possibility to exhibit new optical and electrical properties. The obtained semiconducting hybrid nanomaterials display semiconducting behavior with direct band-to-band transition suggesting applications in field-effect transistors and particularly in photodetector devices without the need for manipulating individual nanoparticles.

## Experimental

**Synthesis of WO<sub>3</sub> nanowires and their conversion to WS<sub>2</sub> nanohybrids.** WO<sub>3</sub> nanowires were synthesized by the hydrothermal method as described in our earlier work<sup>22</sup>. In a typical process, 18.74 g of Na<sub>2</sub>WO<sub>4</sub>·2H<sub>2</sub>O (Sigma-Aldrich, ACS reagent 99%) and 22.49 g of Na<sub>2</sub>SO<sub>4</sub> (Sigma-Aldrich, ACS reagent ≥99.0%) were dissolved in 600 mL distilled water and the pH = 1.5 was adjusted using 3 M HCl solution. After 10 min stirring, the solution was transferred to an autoclave (Parr Series 4520 Bench Top Reactor with PTFE lining) and stirred (35 rpm) for 48 h at 180 °C under autogenic pressure. The product suspension was collected, centrifuged (Hettich, Universal 320, 20 min, 3000 rpm), washed with distilled water and ethanol and then dried at 60 °C for 24 h.

WS<sub>2</sub> nanomaterials were obtained by a sulfurization of the WO<sub>3</sub> nanowires. Sulfur powder (1.0 g, reagent grade, purified by sublimation) and WO<sub>3</sub> nanowires (0.1 g) were placed in two different alumina boats at the center of a tubular reactor (quartz tube of 2" diameter mounted in a 12" single zone Thermolyne, split furnace). Before sulfurization, the reactor was evacuated to a base pressure of ~1 Torr and filled up with N<sub>2</sub> at 1 bar. The evacuation and flushing steps were repeated three times to minimize O<sub>2</sub> in the reactor. Sulfurization is performed for a period of 10 min at 500, 600, 700 or 800 °C in a flow of 400 sccm N<sub>2</sub>. Structural characterization. The crystal phase and microstructure of the obtained material is studied by the means of X-ray diffraction (Bruker D8 Discovery, Cu K<sub>α</sub>), micro-Raman spectroscopy (Horiba Jobin-Yvon Labram HR800 at λ = 488 nm), as well as scanning (FESEM, Zeiss Ultra Plus) and transmission electron microscopy (FEI Tecnai G2 20 X-Twin at 200 kV acceleration) techniques.

**Electrical and optical characterization.** WS<sub>2</sub> nanowire-nanoflake hybrid field-effect devices were fabricated on Si/SiO<sub>2</sub> substrate (thermal oxide thickness 300 nm on p<sup>+</sup>-Si). The source and drain Au microelectrodes (300 nm thick Au sputtered on 45 nm Ti adhesion layer) were defined by photolithography. The WS<sub>2</sub> nanowire and nanoflake hybrids were dispersed in acetone and deposited on the electrodes by drop casting. Temperature dependent current-voltage analysis was performed by probing the chips in a Linkam TMS 94 heating stage in air atmosphere using a computer-controlled Keithley 2636A source meter. The transfer characteristics were measured in a bottom-gated FET arrangement, while the optical properties were analyzed by illuminating the channel of the transistor devices using a standard collimated RGB light-emitting diode (emission centered at 623 nm, 517.5 nm and 466 nm with corresponding luminosity values of 800, 4000 and 900 mcd, respectively; chip-to-diode distance of 5 cm at an illumination angle of ~45°).

## Results and Discussion

The cleaned product of the hydrothermally synthesized nanowires (Fig. 1a) shows a diameter distribution between 270 and 390 nm, while the length of the nanowires varies between 1 and 3 μm. Annealing of the nanowires in the vapor of sulfur does not induce considerable changes of the product morphology except for temperatures 700 °C or above when tiny flakes appear on the surface of the nanowires (Fig. 1b–e). The elemental composition obtained by energy-dispersive X-ray spectroscopy (EDS, Table S1) confirms that the product is transformed into WS<sub>2</sub>. The flakes are linked to the nanowires and look like being partially peeled off from the surface rather than subsequently attached to the nanowires. Although the growth mechanism for WO<sub>3</sub> nanowires is now well understood and has been discussed in literature, the formation of WS<sub>2</sub> nanowire-nanoflake hybrid is not yet clear. Shortly, one dimensional WO<sub>3</sub> forms as follows: Initially a WO<sub>3</sub> crystal nucleus is formed, which is then followed by WO<sub>3</sub> primary prism particle formation due to the presence of Na<sup>+</sup> and/or K<sup>+</sup>, which is present due to the formation of NaCl as byproduct<sup>23</sup>. Further crystal growth then happens along the [001] direction as it is energetically more preferential. The effect of NaCl and sulfate were studied in separate papers also, and both of them were found to serve as directing agent in the growth of one dimensional structures<sup>24,25</sup>. WS<sub>2</sub> nanoflake formation however is less clear. It is believed that any minor mechanical stress caused by the transformation of oxide to sulfide might induce easy sliding and fragmentation of the layered WS<sub>2</sub> sheets. As demonstrated earlier, similar but nanomechanical cleavage of MoS<sub>2</sub> layers from a single crystal using an ultra-sharp W tip may be achieved<sup>26</sup>.

X-ray diffraction indicates the hydrothermally synthesized WO<sub>3</sub> nanowires are of the WO<sub>3</sub> hexagonal crystal phase [PDF 01-075-2187]. In the course of sulfurization however, the diffraction pattern changes particularly when the reaction temperature is increased suggesting the conversion of WO<sub>3</sub> to WS<sub>2</sub>. Comparing the relative intensities of the most intensive reflections, it may be concluded that the WO<sub>3</sub> phase dominates until 500 °C, while at 600 °C and above the hexagonal WS<sub>2</sub> [PDF#841398] phase appears as the major constituent of the samples, with a complete oxide to sulfide transformation occurring at 800 °C. In the course of the reaction, oxygen in the

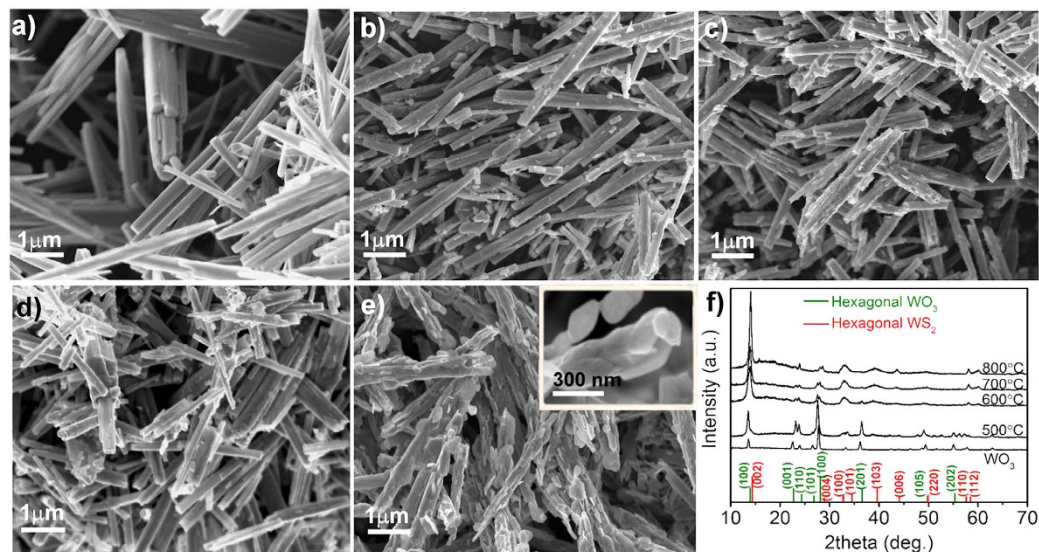


**Figure 1. Structural change of WO<sub>3</sub> during sulfurization.** (a) Scanning electron micrograph of WO<sub>3</sub> nanowires. Panels (b–e) display the corresponding products after sulfurization at 500 °C, 600 °C, 700 °C and 800 °C, respectively. (f) X-ray diffraction patterns of the corresponding products. Note: the reflection located around 24° corresponds to elemental sulfur on the surface of the WS<sub>2</sub>.

anionic sites of the WO<sub>3</sub> crystal is replaced by sulfur resulting in the formation of WS<sub>3</sub>, which then decomposes to WS<sub>2</sub> as  $WS_3 \rightarrow WS_2 + 1/8 S_8^{27}$ .

Since complete transformation of the oxide to sulfide takes place only for the samples treated at 800 °C, the discussion will focus only on this product. High-resolution transmission electron microscopy was performed to observe the morphology and the layer separation in detail (Fig. 2a,b). The measured distance between the fringes in the lattice is approximately 0.62 nm (Fig. 2(b), inset), which matches well the (002) d-spacing for the layered WS<sub>2</sub> structure. Structures were also examined by SAED technique (Fig. 2d), where diffraction patterns revealed crystal structures corresponding to hexagonal WS<sub>2</sub>, which are in good agreement with XRD results. The layered flakes are partially wrapping the nanowires around, demonstrating a kind of exfoliation of the bulk structure. The typical thickness of the flakes is below 10 nm, i.e. the nanostructures consist of up to ~15 layers of WS<sub>2</sub>. XRD (Fig. 1f) and EDS (Table S1) techniques have been used to confirm the formation of the WS<sub>2</sub> nanostructures. First, the sulfur powder turns into vapor carried by the nitrogen and deposited on the surface of the WO<sub>3</sub> nanowire. The high temperature assists the reaction and conversion of the WO<sub>3</sub> nanowire to WS<sub>2</sub> nanowire/nanoflake (substitution of oxygen by sulfur).

Peaks in the micro-Raman spectrum of the sample synthesized at 800 °C (Fig. 2c) can be assigned to the in-plane E<sub>2g</sub> mode (at ~352 cm<sup>-1</sup>) and to the out-of-plane A<sub>1g</sub> mode (at ~420 cm<sup>-1</sup>) of crystalline WS<sub>2</sub>. As reported recently, the intensity ratios and peak frequencies of the WS<sub>2</sub> Raman modes can give information about the number of layers<sup>3,28,29</sup>. In the case of multilayer (>5 layers) WS<sub>2</sub> flakes though, the peak ratios of Raman spectra do not allow the exact determination of layer numbers, as the most prominent change in peak ratios happens at structures having 4 layers or less, as it was discussed by earlier papers. As a result of this, the determined intensity ratio of 0.5 of the peaks for the in-plane E<sub>2g</sub><sup>1</sup> and out-of-plane A<sub>1g</sub> phonon modes can merely confirm that the prepared WS<sub>2</sub> structure is indeed multilayer, which result is also in good agreement with our TEM observations.

Current-voltage curves measured by 2 and 4-probe setups display slightly nonlinear current-voltage characteristics (Fig. 3a). Since the 4-point analysis eliminates any barriers caused by the Au-WS<sub>2</sub> interface, the contacts between the nanohybrids in the random network are also contributing to the contact barriers. Resistance versus temperature measurements (2-probe) carried out in air between 22 °C and 150 °C (Fig. 3b) show a decreasing resistance with temperature indicating a semiconducting behavior of WS<sub>2</sub> nanohybrid films. The two commonly used models to describe the temperature dependence of the resistance of the semiconductors are the thermal-activation and variable range hopping models<sup>12</sup>. In the thermal-activation model, the temperature-dependent resistance can be written as  $R(T) = R_0 e^{(E/kT)}$ , where  $E$  is the activation energy and  $k$  is the Boltzmann constant. The linearized plot (i.e.  $\ln(R)$  vs.  $T^{-1}$ ) gives an excellent fit for our dataset with a reasonable barrier of 0.29 eV obtained from the slope of the fitting parameter, thus thermally activated conduction is a plausible mechanism. Note, the variable range hopping model for 3-dimensional conduction (in which  $\ln(\sigma)$  is linearly proportional to  $T^{-1/4}$ , where  $\sigma$  is the conductivity)<sup>30,31</sup> fits also very well (not displayed here) to our data. However the extracted values for localization length as well as density of electronic states are unphysical thus this latter model for the conduction mechanism may be ruled out.

Although the properties of more common chalcogenides have already been extensively investigated<sup>32–34</sup>, WS<sub>2</sub> nanohybrid materials to our knowledge have not been studied yet. In order to investigate the electrical characteristics of the nanohybrid networks, bottom-gated field-effect devices are prepared on a Si chip of both high and lower synthesis temperature materials. By sweeping the source-drain voltage ( $V_{ds}$ ) between the Au electrodes the current is measured in the WS<sub>2</sub> channel, while a gate voltage ( $V_g$ ) through the conductive Si/Al/Au substrate is

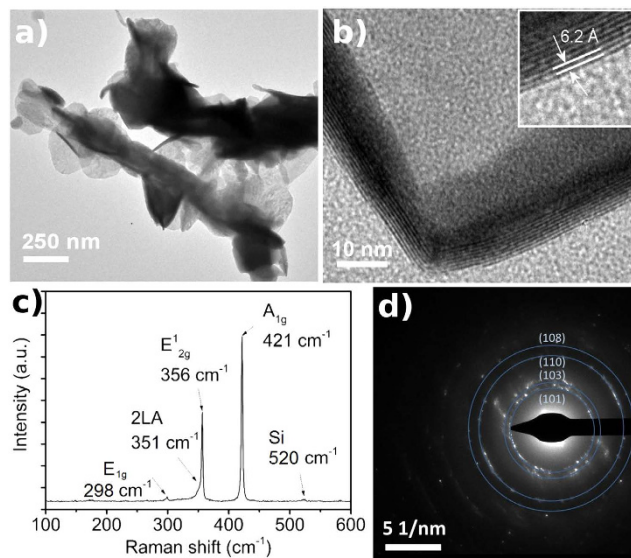


**Figure 2. Structure of WS<sub>2</sub> hybrid materials.** (a) Low magnification transmission electron micrograph of WS<sub>2</sub> nanowire-nanoflake hybrids synthesized at 800 °C. (b) High-resolution micrograph of a flake with layered crystal structure. Inset shows the d-spacing of the layers. (c) Raman spectrum of the corresponding WS<sub>2</sub> nanowire/nanoflake hybrid material. (d) SAED pattern of WS<sub>2</sub> nanowire-nanoflake hybrid synthesized at 800 °C.

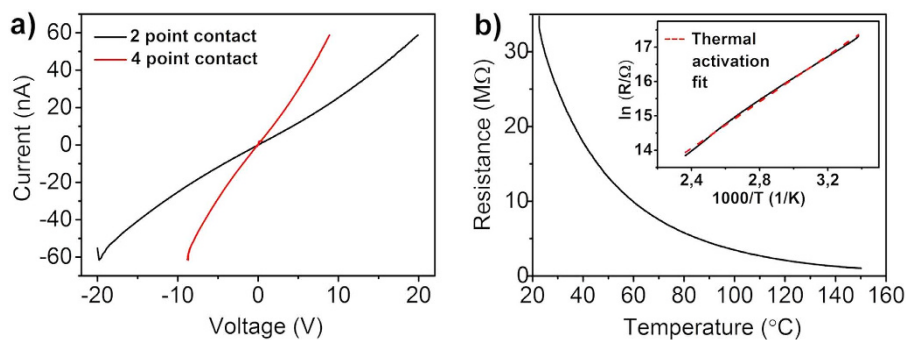


**Figure 3. Electrical characteristics of WS<sub>2</sub> hybrid films.** (a) Current vs. voltage curves measured by 2 and 4-probe setups. (b) Temperature-dependent resistance and the corresponding Arrhenius plot for the thermally activated conduction.

applied. Materials prepared at lower temperatures (500 and 600 °C) exhibited no field effect behavior (Fig. S1), while films made of samples prepared at 800 °C showed a rather weak but measurable field effect. This may be attributed to trapped carriers at the contacts of the nanohybrid particles in the films and also at the interface of the particles and substrate, thus reducing carrier mobility<sup>35</sup>. The field-effect mobility estimated from the conventional two-probe expression<sup>36</sup>  $\mu = \frac{L}{WC_{ox}V_{SD}} \frac{dI_{SD}}{dV_G}$  is about  $\sim 0.02 \text{ cm}^2\text{V}^{-1}\text{s}^{-1}$  (where  $L$  and  $W$  are the channel length and width,  $c_{ox} = \epsilon_0\epsilon_r/d$  is the gate capacitance ( $d = 300 \text{ nm}$  and  $\epsilon_r = 3.9$ ) and  $dI_{SD}/dV_G$  is the transconductance ( $\sim 2.2 \times 10^{-10} \text{ A/V}$ ) estimated from the  $I$ - $V$  slopes measured at different gate voltages (Fig. 4a).

The measured value is comparable with results found for MoS<sub>2</sub> and WS<sub>2</sub> based FETs applying sulfurized metal films ( $0.004$ – $0.04 \text{ cm}^2\text{V}^{-1}\text{s}^{-1}$ )<sup>37,38</sup> and CVD grown MoS<sub>2</sub> from MoO<sub>3</sub> and S precursors ( $0.02 \text{ cm}^2\text{V}^{-1}\text{s}^{-1}$ )<sup>39</sup> or CVD grown WS<sub>2</sub> from WO<sub>3</sub> and S precursors ( $0.01 \text{ cm}^2\text{V}^{-1}\text{s}^{-1}$ )<sup>40</sup>. Some other types of WS<sub>2</sub> materials exhibit higher carrier mobilities due to the smaller number of crystal interconnections as opposed to the smaller nanowire materials where charge needs to pass through a higher number of junctions. Such examples are single crystal WS<sub>2</sub> with  $d \approx 20 \mu\text{m}$  crystal size ( $100 \text{ cm}^2\text{V}^{-1}\text{s}^{-1}$ )<sup>41</sup>, WS<sub>2</sub> films ( $9$ – $15 \text{ cm}^2\text{V}^{-1}\text{s}^{-1}$ )<sup>42</sup>, exfoliated single layer WS<sub>2</sub> ( $80 \text{ cm}^2\text{V}^{-1}\text{s}^{-1}$ )<sup>43</sup> or WS<sub>2</sub> nanotubes ( $50 \text{ cm}^2\text{V}^{-1}\text{s}^{-1}$ )<sup>44</sup>. Taking this into consideration, we speculate that the mobility may be increased by improving the semiconductor-metal contact as well as by using individual (or only a few) WS<sub>2</sub> nanoparticles instead of thick high density random networks between the electrodes, which will result in a smaller number of crystal interconnections between the electrodes.

To verify this assumption, transistors having only a few nanowire-nanoflake hybrid particles connecting the source and drain electrodes were fabricated. The corresponding current-voltage characteristics as shown in Fig. 4(b) are highly nonlinear and have pronounced gate effect owing to the lesser amount of nanohybrid to

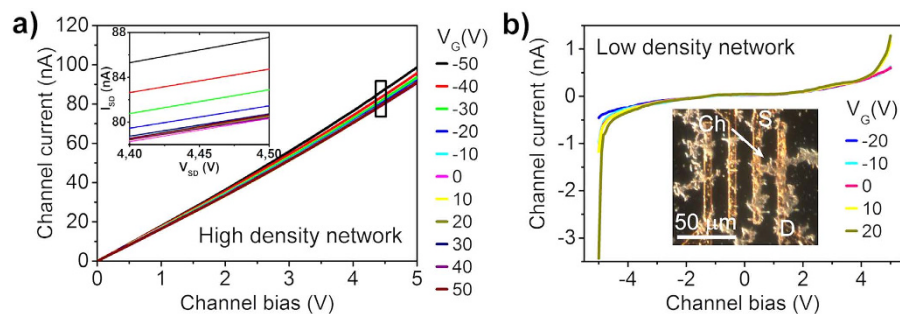


**Figure 4. Output characteristics of the WS<sub>2</sub> nanowire nanoflake hybrid based FET devices.** Current-voltage curves for (a) high and (b) low density random networks of the hybrid nanowires between the source and drain electrodes. Inset in panel (a) displays a magnified plot for the outlined regime between 4.4 and 4.5 V for better visibility of the current values at different gate voltages. Inset in panel (b) shows a dark field optical micrograph of a device.

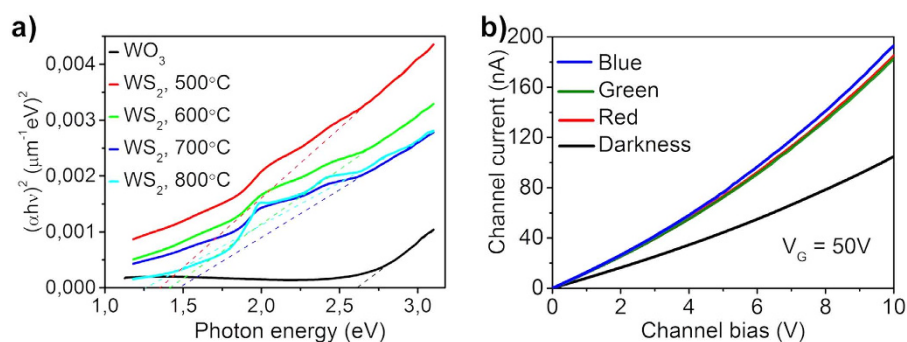


**Figure 5. Optical properties of WS<sub>2</sub> nano hybrids.** (a) Tauc plot for direct band-to-band transition derived from total reflectance measurements on the original and sulfurized powders. Dashed lines represent fitting of the linear sections of each curve. Intersections of the dashed lines with the horizontal axis define the band gap. (b) Current-voltage characteristics of a high density FET under different LED illumination conditions (red, green and blue centered at 623 nm, 517.5 nm and 466 nm, respectively).

nanohybrid contacts in the transistor channel. Unlike in the high-density networks, here the channel has a negative character, as it opens at positive gate voltages. The estimated apparent carrier mobility ( $0.18 \text{ cm}^2 \text{ V}^{-1} \text{ s}^{-1}$ ) of WS<sub>2</sub> in the channel is at least an order of magnitude higher than in the devices with high-density WS<sub>2</sub> nanohybrid networks supporting our hypothesis regarding the performance-limiting effect of excessive numbers of contacts in the films.

Optical measurements of powder samples were carried out to analyze further the properties of the samples. By using a spectrophotometer system (Optronic Laboratories, USA) equipped with an integrating sphere, we measured total reflectance within the 400–1100 nm spectral range from the scattering powders mounted on a microscope slide with double-sided Scotch tape. Then we calculated the optical absorption, from which the band gap of the materials synthesized at various conditions was derived. From the Tauc plot for direct interband transitions (Fig. 5a) we found that the sulfurization results in a clear decrease of the band gap from  $\sim 2.6 \text{ eV}$  to  $\sim 1.4 \text{ eV}$  due to the chemical transformation of tungsten oxide to sulfide. The obtained values are in good agreement with literature values of the band gap for WO<sub>3</sub> after sulfurization<sup>45</sup>.

The photoelectric response of high density network FET devices is studied by illuminating the chips with light-emitting diodes (LEDs) of different color. As displayed in Fig. 5(b), the channel current is found to be increased under illumination using any of the LEDs. However, the effect is somewhat more pronounced when exposing the channel to photons of shorter wavelength due to the better optical absorption and more efficient photogeneration of carriers in the semiconductor. Interestingly, the chip illuminated with the green LED, which is  $\sim 4$ -times brighter than the blue or red source does not cause any extraordinary change in the channel current compared to the other two LEDs. This indicates again that the large contact resistance between the nanowires limits the current and adversely affects the device performance. Anyhow, the magnitude of change in the channel conductance is comparable with those measured for individual single-layer nanoflakes<sup>46</sup>.

## Conclusions

We have synthesized layered semiconducting WS<sub>2</sub> nanowire-nanoflake hybrid materials by a simple sulfurization of WO<sub>3</sub> nanowires at elevated temperatures. Field-effect transistors are demonstrated using bottom gated chips with channel made of random networks of the hybrid material drop casted between source-drain electrodes.

The same structures were also applied as light detectors with good response to visible photons. The performance of both FET and photodetector devices is limited by the large contact resistance between the hybrid nanomaterials in the random network, which may be overcome by using optimized device structures having only a few nanowire-nanoflake hybrid particles in the channel. The work presented here suggests that nanowire-nanoflake hybrids of WS<sub>2</sub>, which can be synthesized by using simple chemical methods in large quantities, are competitive counterparts of few layer chalcogenides in electrical and optoelectronic applications.

## References

- Burda, C., Chen, X., Narayanan, R. & El-Sayed, M. A. Chemistry and properties of nanocrystals of different shapes. *Chem. Rev.* **105**, 1025–1102 (2005).
- Devillanova, F. A. & Du Mont, W. W. Handbook of Chalcogen Chemistry: *New Perspectives in Sulfur, Selenium and Tellurium*. R. Soc. Chem. **1**, 475–513 (2013).
- Akinwande, D., Petrone, N. & Hone, J. Two-dimensional flexible nanoelectronics. *Nat. Commun.* **5**, 5678 (2014).
- Georgiou, T. *et al.* Electrical and optical characterization of atomically thin WS<sub>2</sub>. *Dalton Trans.* **43**, 10388–10391 (2014).
- Iqbal, M. W. *et al.* High-mobility and air-stable single-layer WS<sub>2</sub> field-effect transistors sandwiched between chemical vapor deposition-grown hexagonal BN films. *Sci. Rep.* **5**, 10699 (2015).
- Radisavljevic, B., Radenovic, B., Brivio, A., Giacometti, J. V. & Kis, A. Single-layer MoS<sub>2</sub> transistors. *Nat. Nanotechnol.* **6**, 147–150 (2011).
- Kozawa, D. *et al.* Photocarrier relaxation pathway in two-dimensional semiconducting transition metal dichalcogenides. *Nat. Commun.* **5**, 4543 (2014).
- Wang, Q. H., Kalantar-Zadeh, K., Kis, A., Coleman, J. N. & Strano, M. S. Electronics and optoelectronics of two-dimensional transition metal dichalcogenides. *Nat. Nanotechnol.* **7**, 699–712 (2012).
- Peralta, X. G. *et al.* Terahertz photoconductivity and plasmon modes in double-quantum-well field-effect transistors. *Appl. Phys. Lett.* **81**, 1627–1629 (2002).
- Liu, Z. *et al.* Strain and structure heterogeneity in MoS<sub>2</sub> atomic layers grown by chemical vapour deposition. *Nat. Commun.* **5**, 5246 (2014).
- Nicolosi, V., Chhowalla, M., Kanatzidis, M. G., Strano, M. S. & Coleman, J. N. Liquid exfoliation of layered materials. *Science* **340**, 1226419 (2013).
- Zeng, Z. *et al.* An Effective Method for the Fabrication of Few-Layer-Thick Inorganic Nanosheets. *Angew. Chem. Int. Ed.* **51**, 9052–9056 (2012).
- Zeng, J. *et al.* High yield exfoliation of two-dimensional chalcogenides using sodium naphthalenide. *Nat. Commun.* **5**, 2995 (2014).
- Kuc, A., Zibouche, N. & Heine, T. Influence of quantum confinement on the electronic structure of the transition metal sulfide TS<sub>2</sub>. *Phys. Rev. B* **83**, 245213 (2011).
- Li, H. *et al.* Optical Identification of Single- and Few-Layer MoS<sub>2</sub> Sheets. *Small* **8**, 682–686 (2012).
- Coleman, J. N. *et al.* Two-dimensional nanosheets produced by liquid exfoliation of layered materials. *Science* **331**, 568–571 (2001).
- Chou, S. S. *et al.* Controlling the metal to semiconductor transition of MoS<sub>2</sub> and WS<sub>2</sub> in solution. *J. Am. Chem. Soc.* **137**, 1742–1745 (2015).
- Novoselov, K. S. *et al.* Electric field effect in atomically thin carbon films. *Science* **306**, 666–669 (2004).
- Li, H. Rapid and reliable thickness identification of two-dimensional nanosheets using optical microscopy. *ACS Nano*. **7**, 10344–10353 (2013).
- Liubing, H. *et al.* Synthesis, Characterization and Applications of Cadmium Chalcogenide Nanowires: A Review. *J. Mater. Sci. Technol.* **31**, 556–572 (2015).
- Fang, X. *et al.* ZnS nanostructures: From synthesis to applications. *Prog. Mater. Sci.* **56**, 175–287 (2011).
- Szabó, M. *et al.* Synthesis and characterization of WO<sub>3</sub> nanowires and metal nanoparticle-WO<sub>3</sub> nanowire composites. *J. Mol. Struct.* **1044**, 99–103 (2013).
- Miao, B. *et al.* Large scale hydrothermal synthesis of monodisperse hexagonal WO<sub>3</sub> nanowire and the growth mechanism. *Mater. Lett.* **147**, 12–15 (2015).
- Wang, J., Khoo, E., Lee, P. S. & Ma, J. Synthesis, Assembly, and Electrochromic Properties of Uniform Crystalline WO<sub>3</sub> Nanorods. *J. Phys. Chem. C* **112**, 14306–14312 (2008).
- Wang, X. & Li, Y. Selected-Control Hydrothermal Synthesis of  $\alpha$ - and  $\beta$ -MnO<sub>2</sub> Single Crystal Nanowires. *J. Am. Chem. Soc.* **124**, 2880–2881 (2002).
- Tang, D. M. *et al.* Nanomechanical Cleavage of Molybdenum Disulphide Atomic Layers. *Nat. Commun.* **5**, 3631–3631 (2014).
- van der Vlies, A. J. *Chemical principles of the sulfidation reaction of tungsten oxides* (Doctoral dissertation, Swiss Federal Institute of Technology, Zurich (2002)).
- Berkdemir, A. *et al.* Identification of individual and few layers of WS<sub>2</sub> using Raman Spectroscopy. *Sci. Rep.* **3**, 1755 (2013).
- Zhao, W. *et al.* Lattice dynamics in mono- and few-layer sheets of WS<sub>2</sub> and WSe<sub>2</sub>. *Nanoscale* **5**, 9677–9683 (2013).
- Lin, T. T. *et al.* Variable-Range Hopping and Thermal Activation Conduction of Y-Doped ZnO Nanocrystalline Films. *IEEE Trans. Nanotech.* **13**, 425–430 (2014).
- Pham, T. N. *et al.* Industrially benign super-compressible piezoresistive carbon foams with predefined wetting properties: from environmental to electrical applications. *Sci. Rep.* **4**, 6933 (2014).
- Ghorbani-Asl, M. *et al.* Electromechanics in MoS<sub>2</sub> and WS<sub>2</sub> nanotubes vs. monolayers. *Sci. Rep.* **3**, 2961 (2013).
- Zhu, M. An electrochromic supercapacitor and its hybrid derivatives: quantifiably determining their electrical energy storage by an optical measurement. *J. Mater. Chem. A*. **3**, 21321 (2015).
- Zhu, M. Proton-Insertion-Enhanced Pseudocapacitance Based on the Assembly Structure of Tungsten Oxide. *Appl. Mater. Interfaces* **6**, 18901–18910 (2010).
- Kumar, J., Kuroda, M. A., Bellus, M. Z., Han, S. J. & Chiu, H. Y. Full-range electrical characteristics of WS<sub>2</sub> transistors. *Appl. Phys. Lett.* **106**, 123508 (2015).
- Stallinga, P. & Gomes, H. L. Modeling electrical characteristics of thin-film field-effect transistors: I. Trap-free materials. *Synth. Met.* **156**, 1305–1315 (2006).
- Orofeo, C. M., Suzuki, S., Sekine, Y. & Hibino, H. Scalable synthesis of layer-controlled WS<sub>2</sub> and MoS<sub>2</sub> sheets by sulfurization of thin metal films. *Appl. Phys. Lett.* **105**, 083112 (2014).
- Zhan, Y., Liu, Z., Najmaei, S., Ajayan, P. M. & Lou, J. Large-Area Vapor-Phase Growth and Characterization of MoS<sub>2</sub> Atomic Layers on a SiO<sub>2</sub> Substrate. *Small* **8**, 966–971 (2012).
- Lee, Y. H. *et al.* Synthesis of Large-Area MoS<sub>2</sub> Atomic Layers with Chemical Vapor Deposition. *Adv. Mater.* **24**, 2320–2325 (2012).
- Lee, Y. H. *et al.* Synthesis and transfer of single-layer transition metal disulfides on diverse surfaces. *Nano Lett.* **13**, 1852–1857 (2012).
- Jager-Waldau, A., Lux-Steiner, M. Ch., Jager-Waldau, G. & Bucher, E. WS<sub>2</sub> thin films prepared by sulphurization. *Appl. Surf. Sci.* **70/71**, 731–736 (1993).

42. Tsirlina, T. *et al.* Growth of crystalline WSe<sub>2</sub> and WS<sub>2</sub> films on amorphous substrate by reactive (Van der Waals) rheotaxy. *Sol. Energy Mater. Sol. Cells* **44**, 457–470 (1996).
43. Iqbal, M. W. *et al.* High-mobility and air-stable single-layer WS<sub>2</sub> field-effect transistors sandwiched between chemical vapor deposition-grown hexagonal BN films. *Sci. Rep.* **5**, 10699 (2015).
44. Levi, R., Bitton, O., Leitun, G., Tenne, R. & Joselevich, E. Field-Effect Transistors Based on WS<sub>2</sub> Nanotubes with High Current-Carrying Capacity. *Nano Lett.* **13**, 3736–3741 (2013).
45. Morrish, R., Haak, T. & Wolden, C. A. Low-Temperature Synthesis of *n*-Type WS<sub>2</sub> Thin Films via H<sub>2</sub>S Plasma Sulfurization of WO<sub>3</sub>. *Chem. Mater.* **26**, 3986–3992 (2014).
46. Hwang, W. S. *et al.* Transistors with chemically synthesized layered semiconductor WS<sub>2</sub> exhibiting 10<sup>5</sup> room temperature modulation and ambipolar behavior. *Appl. Phys. Lett.* **101**, 013107 (2012).

### Acknowledgements

The financial support received from OTKA (projects K 112531 and NN 110676), Oulu University Graduate School (Infotech programme), Academy of Finland (projects Optifu, HyNa and Suplacat), EU-FP7 (projects Susfoflex and HiPPoCaMP) are acknowledged.

### Author Contributions

The experiments were carried out by G.A. (materials synthesis, XRD, Raman, EDS and SEM analysis as well as electrical and photoresponse measurements), A.P. (optical measurements) and by R.P. (electrical and HR-TEM analysis) with the assistance of A.D., T.S., J.-F.L. and G.T. The experiments were planned by K.K. The results were discussed by G.A., A.P., J.-F.L., K.K., A.K., Z.K., G.S.L., M.M. and A.L.-S. The manuscript was written by G.A., R.P. and K.K. with the kind help of the co-authors.

### Additional Information

**Supplementary information** accompanies this paper at <http://www.nature.com/srep>

**Competing financial interests:** The authors declare no competing financial interests.

**How to cite this article:** Alene, G. *et al.* A novel WS<sub>2</sub> nanowire-nanoflake hybrid material synthesized from WO<sub>3</sub> nanowires in sulfur vapor. *Sci. Rep.* **6**, 25610; doi: 10.1038/srep25610 (2016).



This work is licensed under a Creative Commons Attribution 4.0 International License. The images or other third party material in this article are included in the article's Creative Commons license, unless indicated otherwise in the credit line; if the material is not included under the Creative Commons license, users will need to obtain permission from the license holder to reproduce the material. To view a copy of this license, visit <http://creativecommons.org/licenses/by/4.0/>